

Communication

Efficient 1054 nm Raman Random Fiber Laser

Pan Wang, Shengtao Lin, Jiaojiao Zhang, Xingyu Bao, Longqun Ni, Yifei Qi and Zinan Wang * 

Key Laboratory of Optical Fiber Sensing and Communications, University of Electronic Science and Technology of China, Chengdu 611731, China

* Correspondence: znwang@uestc.edu.cn

Abstract: Low-coherence laser is regarded as the key to mitigating laser-plasma instability (LPI) in laser-driven inertial confinement fusion (ICF), where LPI can decrease the laser energy coupled to the target. With the merits of low coherence, high spectral stability, and flexible output characteristics, the Raman random fiber laser (RRFL) is considered to be a candidate light source in ICF. In this paper, the 1054 nm RRFL with high slope efficiency is achieved for the first time. In the RRFL pump source design section, we have optimized the ytterbium-doped fiber (YDF) length by simulation and amplified the power by Master Oscillator Power Amplifier (MOPA) to realize a 1011 nm YDF laser with 47.3 dB optical signal-to-noise ratio (OSNR). In terms of RRFL cavity design, a fiber loop mirror and Rayleigh scattering in the HI 1060 Flex fiber provide wideband point feedback and random distributed feedback, respectively. Based on this system, we achieve an RRFL output with 0.4 nm half-maximum full width, 182% slope efficiency, and 41.3 dB OSNR. This work will provide guidance for the application of RRFL in high-energy-density physics research.

Keywords: random distributed feedback fiber laser; Raman gain; ytterbium-doped fiber laser

1. Introduction

In laser-driven inertial confinement fusion (ICF) and other areas of high energy density physics, there is a critical issue that laser-plasma instability (LPI) can cause laser energy loss and even reduce the fusion reaction capacity [1,2]. The low-coherence laser is considered to be one of the most effective methods to overcome the effects of LPI [3,4], and important research results have been obtained, mainly with amplified spontaneous emission (ASE) sources [5–8]. However, these schemes involve complex spectral modulation and amplification processes. Therefore, a new low-coherence light source is urgently needed. Random fiber laser (RFL) is based on random distributed feedback [9], which is able to match the gain band of the ICF amplification system via a simple cavity structure design. Further, RFL has great potential for intracavity time domain modulation and coherent characteristic modulation [10,11]. Therefore, RFL is considered one of the candidate seed sources for the next generation of ICF.

Due to the gain band of the ICF amplification system having a 3-dB free-oscillation spectrum in the range 1051.7~1054.5 nm, the research on ~1.05 μm RFL for ICF has attracted a lot of attention [12]. The 1053 nm ytterbium-doped RFL (YRFL) has been experimentally demonstrated [12,13]. Fan et al. utilized a 9.5 m ytterbium-doped fiber (YDF) and a 2 km single-mode fiber (SMF) to achieve a 1053 nm YRFL with the 0.48 nm full width at half-maximum (FWHM), which has the potential to be a laser source in large high-energy laser devices [13]. In the latest study of RFL for ICF, the new record of RFL with 28 mJ pulse energy and megawatt-class peak power was reached utilizing a forward-pumped 1053 nm YRFL with 2.5 nm FWHM as the seed source [12]. However, the YRFL with a broadband spectrum will lead to instability in the output spectrum due to mode competition and other non-linear effects. To solve the issues, the Raman fiber random laser (RRFL) can be exploited in ICF, with the advantages of spectral domain stability and high



Citation: Wang, P.; Lin, S.; Zhang, J.; Bao, X.; Ni, L.; Qi, Y.; Wang, Z. Efficient 1054 nm Raman Random Fiber Laser. *Photonics* **2023**, *10*, 851. <https://doi.org/10.3390/photonics10070851>

Received: 26 May 2023
Revised: 30 June 2023
Accepted: 20 July 2023
Published: 22 July 2023



Copyright: © 2023 by the authors. Licensee MDPI, Basel, Switzerland. This article is an open access article distributed under the terms and conditions of the Creative Commons Attribution (CC BY) license (<https://creativecommons.org/licenses/by/4.0/>).

slope efficiency [14–17]. In addition, the influence of the photodarkening effect in the YDF is avoided in RRFL.

RRFL, utilizing stimulated Raman scattering in passive fiber as the gain, has the benefits of broadband output, high slope efficiency, effective amplification, high stability [18–24], etc. In terms of broadband output and stability, Zhou et al. achieved a stable 1150 nm RRFL with ~7 nm FWHM, pumped by a 1090 nm ytterbium-doped fiber laser (YDFL) [18].

The stable RRFL outputs at 1174 nm, 1240 nm, 1310 nm, and 1390 nm were realized by 1117 nm YDFL pumping multi-element fiber Bragg grating (FBG) and different lengths of standard coupler fiber. The FWHM of RRFL is 7.3 nm, 6.3 nm, 8.6 nm, and 8.6 nm, respectively [19]. The 1055 nm polarized YDFL pumped polarization-maintaining fiber, implementing a stable 1107 nm polarized RRFL with 5.24 nm FWHM [20]. For the superiority of slope efficiency in RRFL, Wang et al. generated a stable 1140 nm RRFL with slope efficiency over 200% and ~3 nm FWHM, based on the half-open cavity [21]. The 1064 nm YDFL pumped half-open cavity with 30 m phosphosilicate fiber, producing a stable 1238 nm RRFL with 7.1 nm FWHM and ~130% slope efficiency [22]. Based on large-mode-area germanium-doped fibers, a quasi-kilowatt stable 1150 nm RRFL output with ~7 nm FWHM and 152% slope efficiency was generated [18]. In the aspect of effective amplification, Xiao et al. utilized a 1064 nm RRFL as the seed source, which was amplified from 8.66 W to 4020 W by a Master Oscillator Power Amplifier (MOPA) configuration, resulting in the 4-kW level stable output [23]. A 1070 nm RRFL with 6.5 W power acted as the seed source and was amplified by a two-stage MOPA to reach a 5.1 kW level stable output [24]. In particular, the RRFL has been demonstrated to be an effective seed source for power amplification in the field of high-power fiber laser facilities [25,26]. However, the RRFL at ~1.05 μm band has not been reported owing to the lack of a suitable high-power pumping source.

To generate the 1054 nm RRFL, the pumping wavelength should be around 1011 nm correspondingly. In general, RRFL operating at the ~1 μm band requires a YDFL as the pumping source [27]. In a YDF, the gain at 1011 nm is much less than the gain at the 1020–1040 nm range [28,29]. Thus, unstable ASE often occurs at around 1030 nm, which causes great difficulty in generating 1011 nm YDFL [30,31]. The unstable ASE will lead to turbulent laser output and may even damage fiber optic components. According to recent research, the occurrence of ASE around 1030 nm is not only related to the length of the YDF but also to the cavity mirror reflexivity [32,33]. Moreover, the 1011 nm laser power can be further amplified by adding a classical MOPA configuration [34–36]. Therefore, it is necessary to delicately design a scheme that can effectively suppress the ASE and achieve high power 1011 nm laser output.

In this paper, a 1054 nm RRFL with a stable spectrum and high slope efficiency is proposed for the first time. In the 1054 nm RRFL system, the pumping source is the specially designed 1011 nm YDFL, and the cavity consists of passive HI 1060 Flex fiber and fiber loop mirror (FLM). In the investigation of a high-power 1011 nm YDFL scheme, the appropriate YDF length is determined by simulation, and the laser power is amplified by a MOPA configuration. Based on this pump, the 1054 nm RRFL achieves a stable spectrum with 0.4 nm FWHM and 182% slope efficiency, and the lasing threshold is around 0.66 W.

2. Simulation and Experimentation of YDFL

In this chapter, we simulate the steady rate equations of cladding-pumped YDFL to determine a 1011 nm YDFL scheme and demonstrate it experimentally. Furthermore, the results of the simulation and experiment are analyzed.

2.1. Simulation of YDFL

The laser output spectrum can be simulated using the steady rate equations of cladding-pumped YDFL. The steady rate equations consider the geometric parameters of the active fiber (core/cladding diameter, length), as well as various wavelength-related parameters such as absorption cross-section, emission cross-section, cavity mirror re-

flectivity, etc. The YDFL spectrum is simulated by calculating the following steady rate equations [37]:

$$\frac{N_2(z)}{N} = \frac{\frac{(P_p^+(z)+P_p^-(z))\sigma_a(\lambda_p)\Gamma_p}{h\nu_p A} + \sum_k \frac{(P^+(z,\lambda_k)+P^-(z,\lambda_k))\sigma_a(\lambda_k)\Gamma_s}{h\nu_k A}}{\frac{(P_p^+(z)+P_p^-(z))(\sigma_a(\lambda_p)+\sigma_e(\lambda_p))\Gamma_p}{h\nu_p A} + \frac{1}{\tau} + \sum_k \frac{(P^+(z,\lambda_k)+P^-(z,\lambda_k))(\sigma_a(\lambda_k)+\sigma_e(\lambda_k))\Gamma_s}{h\nu_k A}} \quad (1)$$

$$\pm \frac{dP_p^\pm(z)}{dz} = -\Gamma_p [\sigma_a(\lambda_p)N - (\sigma_a(\lambda_p) + \sigma_e(\lambda_p))N_2(z)]P_p^\pm(z) - \alpha(\lambda_p)P_p^\pm(z) \quad (2)$$

$$\pm \frac{dP^\pm(z,\lambda_k)}{dz} = \Gamma_s[(\sigma_a(\lambda_k) + \sigma_e(\lambda_k))N_2(z) - \sigma_a(\lambda_k)N]P^\pm(z,\lambda_k) + 2\Gamma_s\sigma_e(\lambda_k)N_2(z)\frac{hc^2}{\lambda_k^3}\Delta\lambda - \alpha(\lambda_k)P^\pm(z,\lambda_k) + \varepsilon(\lambda_k)P^\mp(z,\lambda_k) \quad (3)$$

Here, N is Yb^{3+} ion concentration and N_2 represents the excited state population. $P(z, \lambda_k)$ demonstrates the power of wavelength λ_k at position z . The subscript ‘ k ’ corresponds to different wavelengths. The subscript ‘ p ’ and ‘ s ’ represent pump and signal. Γ_p and Γ_s are the pump and signal to overlap within the core, respectively. σ_a and σ_e are the absorption and emission cross sections for the YDF. A and α mean the core area and attenuation of the YDF, respectively. τ is the Yb^{3+} ion lifetime. ε is Rayleigh scattering coefficient. The simulation parameters are listed in Table 1 [12,13].

Table 1. Simulation parameters for YDF.

Parameters	Pump	Emission
λ (nm)	976	1011
σ_a (m ²)	2.476×10^{-24}	8.634×10^{-26}
σ_e (m ²)	2.483×10^{-24}	4.488×10^{-25}
α (m ⁻¹)	0.006	0.005
Γ	0.0064	0.9
h		6.626×10^{-34}
A (m ²)		7.854×10^{-11}
τ (ms)		0.8

The laser output spectra with different YDF lengths are simulated, as shown in Figure 1. Here, the high reflectivity FBG (HR-FBG) and low reflectivity FBG (LR-FBG) are 99% and 15%, respectively. When YDF length is 0.9 m, the expected 1011 nm laser is significantly higher than ASE near 1030 nm. Moreover, it demonstrates an excellent optical signal-to-noise ratio (OSNR). When the YDF length is 1.2 m, ASE accounts for almost all the output power.

2.2. Experimentation of YDFL

Furthermore, experiments are conducted based on the simulation results, and the experimental setup is shown in Figure 2. The YDFL is cladding-pumped by a 976 nm laser diode (LD1) in a laser cavity combining a YDF (Nufern LMA-YDF-10/130) and a pair of 1011 nm FBGs. The reflectivity of the FBGs is 99% (HR-FBG) and 15% (LR-FBG), respectively. The signal port of the combiner is connected to the HR-FBG, and the output port is connected to a YDF. The cladding power stripper (CPS) plays a role in removing residual pump and mode-field adaptation. Then, the output of YDFL is filtered by a 1011 nm FBG to obtain the pure 1011 nm laser.

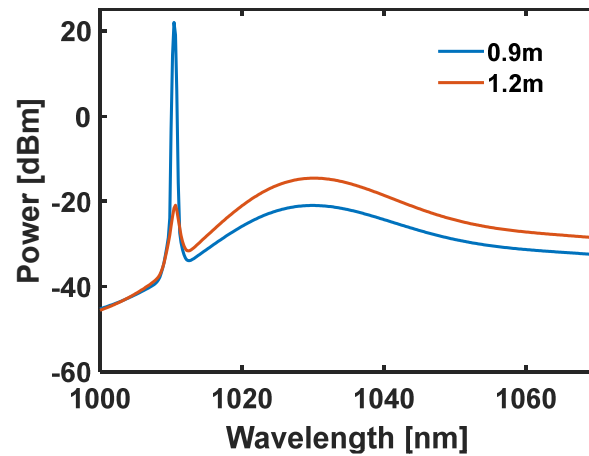


Figure 1. Simulated laser output spectra with different YDF lengths.

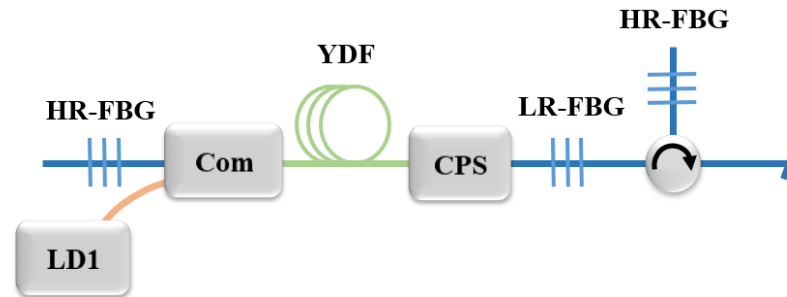


Figure 2. Experimental setup of the 1011 nm YDFL. Com: combiner; CPS: cladding power stripper.

The spectra are measured by an optical spectrum analyzer (OSA) with 0.01 nm resolution. Figure 3 shows the output spectra of YDFL with different YDF lengths. Consistent with the simulation results, the 1011 nm laser with 0.9 m YDF has 40.8 dB OSNR, and ASE is effectively suppressed. However, the output is unstable ASE and contains almost no 1011 nm laser by using 1.2 m YDF. Therefore, a 0.9 m YDF is used in the following experiments. In addition, the filtered 1011 nm YDFL output spectrum is shown in the insert of Figure 4. In this case, the output 1011 nm laser power as a function of LD1 pump power is illustrated in Figure 4. When the pump power is 4 W, the pure 1011 nm laser power is 0.22 W. The YDFL requires further design to provide higher pumping power for the 1054 nm RRFL.

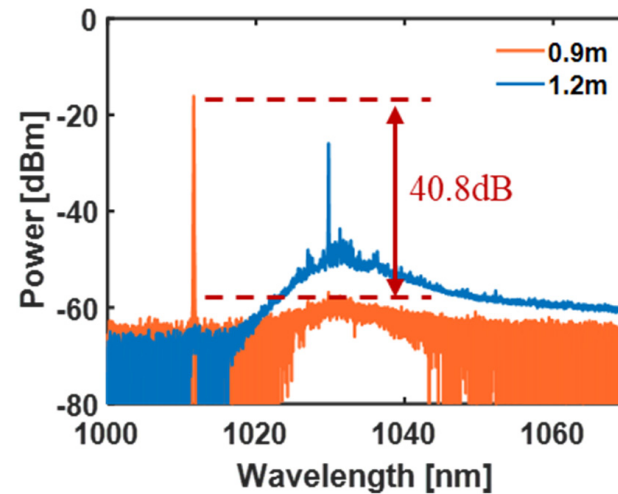


Figure 3. YDFL output spectra with different YDF lengths.

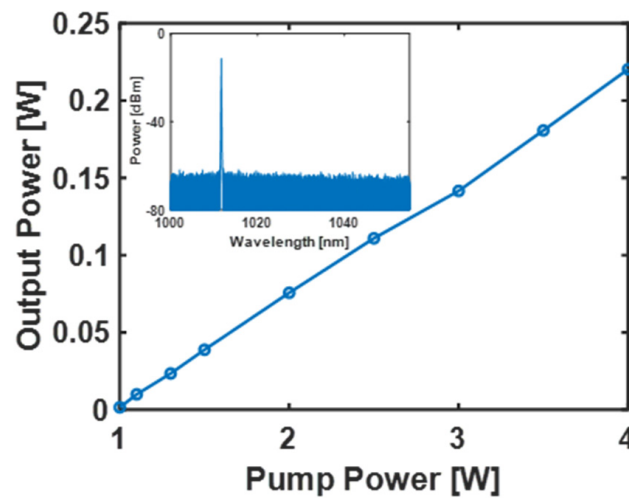


Figure 4. Output power of the 1011 nm laser vs. LD1 pump power. Insert: the spectrum of filtered 1011 nm YDFL.

3. Experiments and Results of RRFL

In this chapter, we prove that an effective 1.05 μm RRFL with stable spectral output can be implemented based on the specially designed 1011 nm YDFL. Based on the experimental setup shown in Figure 5, the experimental results of MOPA and RRFL are presented and analyzed.

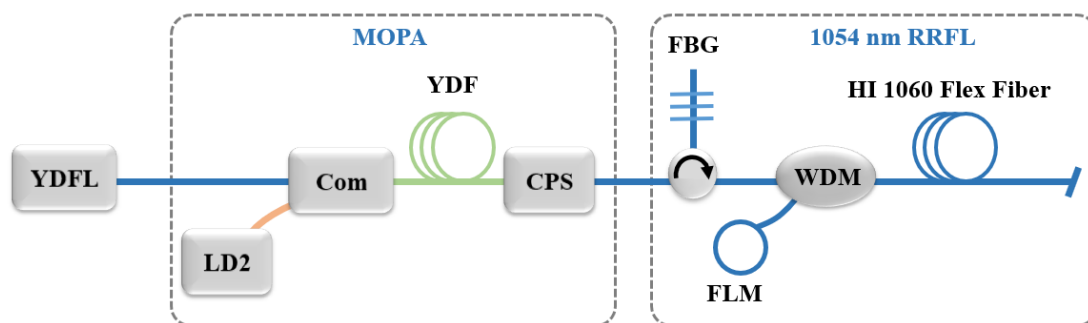


Figure 5. Experimental setup of the RRFL. LD2: 976 nm laser diode; Com: combiner; CPS: cladding power stripper; FBG: 1011 nm fiber Bragg grating; WDM: wavelength division multiplexer; FLM: fiber loop mirror.

3.1. Experimental Setup

Figure 5 shows the experimental setup of Raman random fiber lasing generation pumped by the specially designed 1011 nm YDFL. The experimental scheme mainly consists of two parts: MOPA and 1054 nm RRFL. The 1011 nm YDFL is further amplified in a MOPA configuration with a 0.9 m YDF. The YDFL is launched into the power scaling amplifier via a combiner. The pump source of the amplifier comes from LD2 at 976 nm. The amplified YDFL is used as the pump source for the RRFL and is injected into the 1011 nm port of the wavelength division multiplexer (WDM). The 1054 nm port of the WDM is attached to an FLM, providing wideband point feedback for Raman random lasing. The common port of the WDM is spliced with a 3 km passive HI 1060 Flex fiber to provide the Raman gain and random distributed Rayleigh backscattering. In order to generate stable ~1.05 μm Raman random lasing and avoid the transverse mode competition effect, the HI 1060 Flex fiber with 930 nm cut-off wavelength is used here rather than the standard communication fiber with ~1.3 μm cut-off wavelength. Furthermore, the efficient 1054 nm RRFL is realized via a forward-pumping short cavity structure.

3.2. MOPA

The YDFL is further amplified via a MOPA configuration, and the output characteristics of the 1011 nm amplifier are investigated. Figure 6 shows the output spectra of the 1011 nm amplifier at different pump powers when the YDFL power is 0.22 W. The results indicate that the 1011 nm amplifier still performs excellent ASE suppression with increasing pump power and achieves over 47 dB OSNR when the YDFL power is fixed.

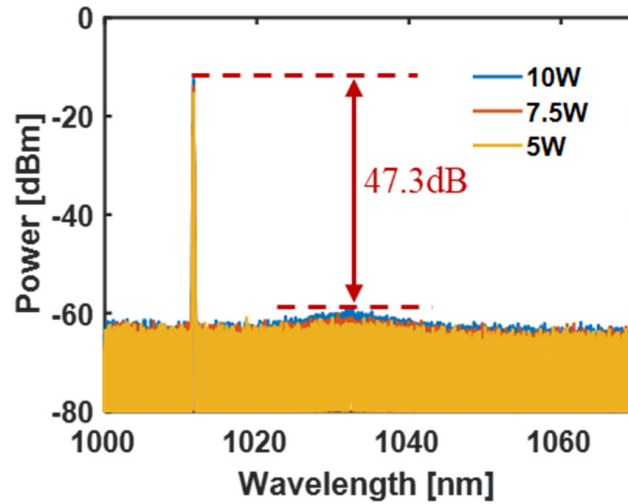


Figure 6. Spectra of the 1011 nm amplifier at different pump powers.

Figure 7a illustrates the spectra of the 1011 nm amplifier when the pump power is 7.5 W and YDFL powers are 0.22 W, 0.14 W, and 0.07 W, respectively. The details of the peak region are shown in the insert of Figure 7a. The intensity of ASE is inversely proportional to the 1011 nm laser power, indicating that higher seed laser power is beneficial for suppressing ASE. The output power of the 1011 nm amplifier at different YDFL powers versus LD2 pump power is shown in Figure 7b. The slope efficiency of the three curves are 16.57%, 15.95%, and 15%, respectively, corresponding to YDFL power of 0.22 W, 0.14 W, and 0.07 W. The slope efficiency difference of the three curves is due to the different weights of ASE power, as can be observed in Figure 6. Therefore, the 0.22 W YDFL power is used during the subsequent experiments.

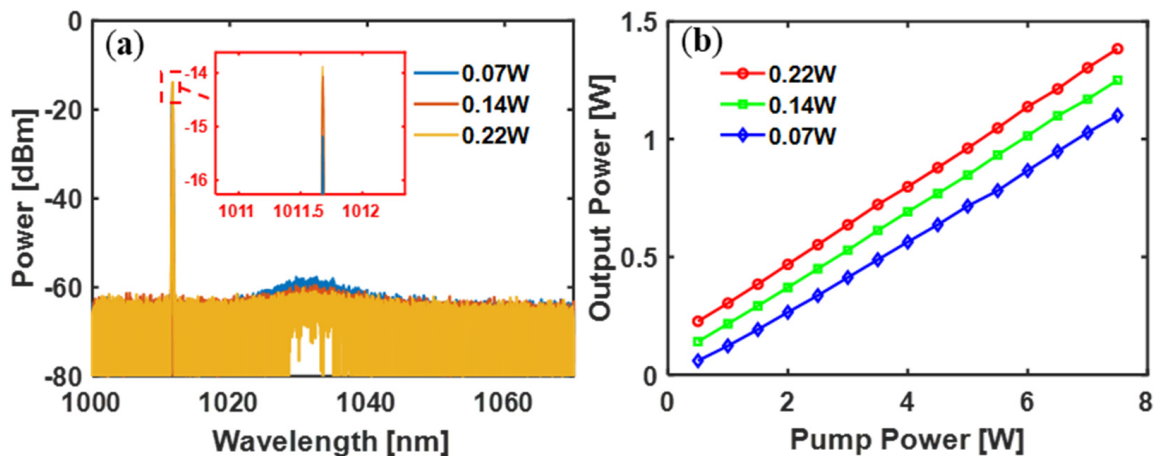


Figure 7. (a) Spectra of the 1011 nm amplifier at different YDFL powers. Insert: local amplification in the peak region. (b) Output power of the 1011 nm amplifier at different YDFL powers vs. LD2 pump power.

3.3. RRFL

The effective 1054 nm RRFL is realized using a forward-pumping half-open cavity structure. The 1054 nm RRFL spectrum and the 3 km HI 1060 Flex passive fiber Raman gain spectrum are shown in Figure 8. The 1054 nm RRFL spectrum has 0.4 nm FWHM and 41.3 dB OSNR. Due to the Raman gain spectrum, the 1054 nm RRFL spectrum has a bottom shape.

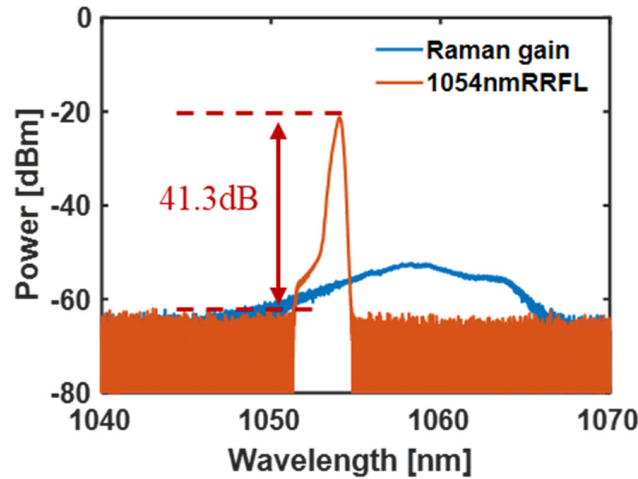


Figure 8. The 1054 nm RRFL spectrum and the 3 km HI 1060 Flex passive fiber Raman gain spectrum.

A 10 MHz photodetector and a 16 GHz oscilloscope are used to measure the relative intensity noise (RIN) of 1054 nm RRFL. The RIN of 1054 nm RRFL is shown in Figure 9a. There are no resonance peaks observed with the $c/2nL \sim 33.3$ kHz spacing corresponding to cavity length. This fact demonstrates the random characteristics of the laser output. However, a clear mode structure with a spacing of 61 kHz is observed in the low-frequency region, as shown in the insert of Figure 9a. Using the same measurement devices, the RIN of 976 nm LD1 is measured, as shown in Figure 9b. The results indicate that the resonance peaks with 61 kHz spacing in the low-frequency region of 1054 nm RRFL are transmitted by LD1.

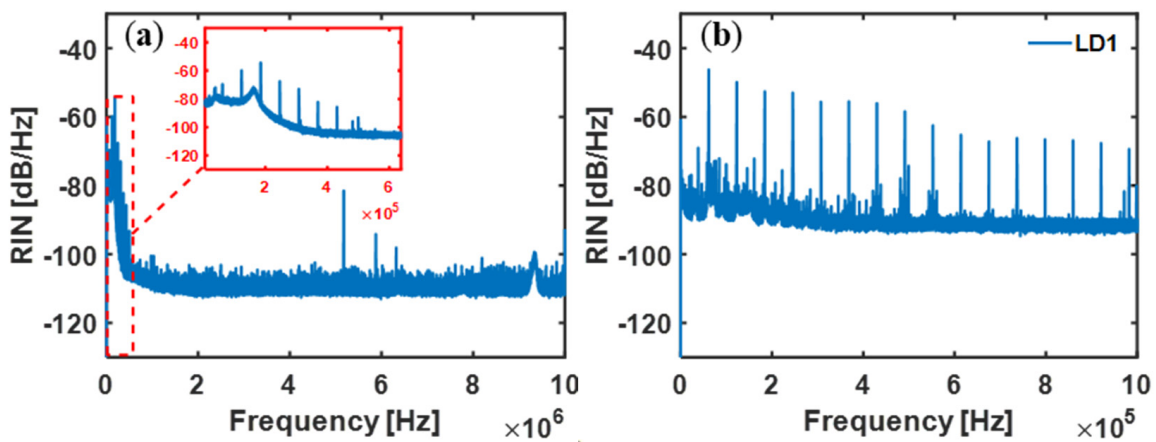


Figure 9. The RIN of (a) 1054 nm RRFL and (b) 976 nm LD1. Insert: local amplification in the low-frequency region.

Figure 10 shows the output of 1054 nm RRFL power at the fiber end as a function of 1011 nm YDFL pump power. The 1054 nm RRFL has a lasing threshold of around 0.66 W and a slope efficiency of 182%. The pump power can be efficiently converted to output laser power, and 56% optical conversion efficiency can be obtained at 0.87 W pump power. Compared with existing research results about $\sim 1.05 \mu\text{m}$ RFL, the optical conversion

efficiency is 38% and 32%, respectively, in realizing a 1053 nm YRFL based on forward and backward pumping structure [13]. The optical conversion efficiency is ~9.5% when implementing a broadband 1053 nm YRFL [12]. The experimental results show that the system can generate an efficient 1054 nm RRFL.

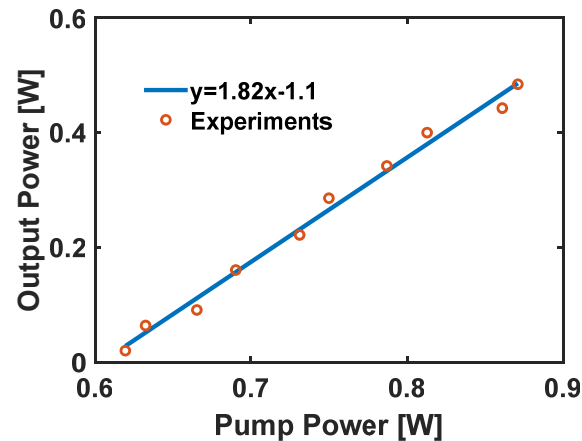


Figure 10. Output power of the 1054 nm RRFL vs. 1011 nm YDFL pump power.

4. Conclusions

In this paper, we have demonstrated a 1054 nm RRFL with high slope efficiency for the first time, based on the specially designed 1011 nm YDFL pump. We delicately investigate the scheme of 1011 nm YDFL based on simulation. Furthermore, the laser power is amplified by the MOPA configuration, and the amplification output characteristics are demonstrated. The specially designed 1011 nm YDFL output can reach 1.78 W and 47.3 dB OSNR. In the 1054 nm RRFL, the specially designed 1011 nm YDFL is used to pump the passive HI 1060 Flex fiber. As a result, the 1054 nm RRFL achieves a stable spectrum with 0.4 nm FWHM and 182% slope efficiency.

In further work, this design scheme for 1011 nm YDFL will provide references for other pump sources around 1 μm . Moreover, this work can help RFL to develop application potential in high-power laser drivers.

Author Contributions: Conceptualization, P.W., S.L. and Z.W.; methodology, P.W., S.L. and Z.W.; validation, P.W., S.L., J.Z., X.B., L.N. and Y.Q.; resources, Z.W.; writing—original draft preparation, P.W.; writing—review and editing, P.W., S.L., J.Z., X.B., L.N., Y.Q. and Z.W.; supervision, Z.W.; project administration, Z.W.; funding acquisition, Z.W. All authors have read and agreed to the published version of the manuscript.

Funding: This research was funded by the Natural Science Foundation of China (62075030) and the 111 Project (B14039).

Institutional Review Board Statement: Not applicable.

Informed Consent Statement: Not applicable.

Data Availability Statement: The data underlying the results presented in this paper are not publicly available at this time but may be obtained from the authors upon reasonable request.

Conflicts of Interest: The authors declare no conflict of interest.

References

1. Labaune, C. Incoherent light on the road to ignition. *Nat. Phys.* **2007**, *3*, 680–682. [[CrossRef](#)]
2. Lindl, J.; Landen, O.; Edwards, J.; Moses, E.; NIC Team. Review of the National Ignition Campaign 2009–2012. *Phys. Plasmas* **2014**, *21*, 020501. [[CrossRef](#)]
3. Obenschain, S.P.; Luhmann, N.C.; Greiling, P.T. Effects of finite-bandwidth driver pumps on the parametric-decay instability. *Phys. Rev. Lett.* **1976**, *36*, 1309–1312. [[CrossRef](#)]

4. Mostovych, A.N.; Obenschain, S.P.; Gardner, J.H.; Grun, J.; Kearney, K.J.; Manka, C.K.; McLean, E.A.; Pawley, C.J. Brillouin scattering measurements from plasmas irradiated with spatially and temporally incoherent laser light. *Phys. Rev. Lett.* **1987**, *59*, 1193–1196. [[CrossRef](#)]
5. Rao, D.X.; Gao, Y.Q.; Cui, Y.; Ji, L.L.; Zhao, X.H.; Liu, J.; Liu, D.; Li, F.J.; Shan, C.; Shi, H.T.; et al. 1 μ s nanosecond low-coherent laser source with precise temporal shaping and spectral control. *Opt. Laser Technol.* **2020**, *122*, 105850. [[CrossRef](#)]
6. Dorrer, C.; Spilatro, M. Spectral and temporal shaping of spectrally incoherent pulses in the infrared and ultraviolet. *Opt. Express* **2022**, *30*, 4942–4953. [[CrossRef](#)] [[PubMed](#)]
7. Cui, Y.; Gao, Y.Q.; Rao, D.X.; Liu, D.; Li, F.J.; Ji, L.L.; Shi, H.T.; Liu, J.N.; Zhao, X.H.; Feng, W.; et al. High-energy low-temporal-coherence instantaneous broadband pulse system. *Opt. Lett.* **2019**, *44*, 2859–2862. [[CrossRef](#)]
8. Dorrer, C.; Hill, E.M.; Zuegel, J.D. High-energy parametric amplification of spectrally incoherent broadband pulses. *Opt. Express* **2020**, *28*, 451–471. [[CrossRef](#)]
9. Turitsyn, S.K.; Babin, S.A.; Atalla, E.T.; Harper, P.; Churkin, D.V.; Kablukov, S.I.; Ania-Castañón, J.D.; Karalekas, V.; Podivilov, E.V. Random distributed feedback fibre laser. *Nat. Photonics* **2010**, *4*, 231–235. [[CrossRef](#)]
10. Bravo, M.; Fernandez-Vallejo, M.; Lopez-Amo, M. Internal modulation of a random fiber laser. *Opt. Lett.* **2013**, *38*, 1542–1544. [[CrossRef](#)]
11. Wu, H.; Han, B.; Wang, Z.N.; Liang, H.K. Statistical properties of Er/Yb co-doped random Rayleigh feedback fiber laser. *Chin. Opt. Lett.* **2021**, *19*, 021402. [[CrossRef](#)]
12. Fan, M.Q.; Lin, S.T.; Yao, K.; Qi, Y.F.; Zhang, J.J.; Zheng, J.W.; Wang, P.; Ni, L.Q.; Bao, X.Y.; Zhou, D.D.; et al. Spectrum-tailored random fiber laser towards ICF laser facility. *Matter Radiat. Extrem.* **2023**, *8*, 025902. [[CrossRef](#)]
13. Fan, M.Q.; Zon, Z.Y.; Tian, X.C.; Xu, D.P.; Zhou, D.D.; Zhang, R.; Zhu, N.; Xie, L.H.; Li, H.X.; Su, J.Q.; et al. Comprehensive Investigations on 1053 nm Random Distributed Feedback Fiber Laser. *IEEE Photonics J.* **2017**, *9*, 1–9. [[CrossRef](#)]
14. Lin, S.T.; Wang, Z.N.; Araújo, H.A.; Raposo, E.P.; Gomes, A.S.L.; Wu, H.; Fan, M.Q.; Rao, Y.J. Ultrafast convergent power-balance model for Raman random fiber laser with half-open cavity. *Opt. Express* **2020**, *28*, 22500–22510. [[CrossRef](#)]
15. Han, B.; Dong, S.S.; Liu, Y.; Wang, Z.N. Cascaded Random Raman Fiber Laser with Low RIN and Wide Wavelength Tunability. *Photonic Sens.* **2022**, *12*, 220414. [[CrossRef](#)]
16. Lin, S.T.; Wang, Z.N.; Zhang, J.J.; Wang, P.; Wu, H.; Qi, Y.F. Radiation build-up and dissipation in Raman random fiber laser. *Sci. China Inf. Sci.* **2022**. [[CrossRef](#)]
17. Wang, Z.N.; Wu, H.; Fan, M.Q.; Rao, Y.J.; Jia, X.H.; Zhang, W.L. Third-order random lasing via Raman gain and Rayleigh feedback within a half-open cavity. *Opt. Express* **2013**, *21*, 20090–20095. [[CrossRef](#)]
18. Zhang, H.W.; Huang, L.; Song, J.X.; Wu, H.; Zhou, P.; Wang, X.L.; Wu, J.; Xu, J.M.; Wang, Z.N.; Xu, X.J.; et al. Quasi-kilowatt random fiber laser. *Opt. Lett.* **2019**, *44*, 2613–2616. [[CrossRef](#)]
19. Grimes, A.; Hariharan, A.; Sun, I.; Nicholson, J.W. High-power, high-efficiency, semi-random Raman fiber lasers. *Fiber Lasers XIX Technol. Syst.* **2022**, *11981*, 137–141.
20. Ye, J.; Xu, J.M.; Song, J.X.; Wu, H.S.; Zhang, H.W.; Wu, J.; Zhou, P. Flexible spectral manipulation property of a high power linearly polarized random fiber laser. *Sci. Rep.* **2018**, *8*, 2173. [[CrossRef](#)]
21. Wang, Z.N.; Wu, H.; Fan, M.Q.; Zhang, L.; Rao, Y.J.; Zhang, W.L.; Jia, X.H. High power random fiber laser with short cavity length: Theoretical and experimental investigations. *IEEE J. Sel. Top. Quantum Electron.* **2014**, *21*, 10–15. [[CrossRef](#)]
22. Dong, J.Y.; Zhang, L.; Zhou, J.Q.; Pan, W.W.; Gu, X.J.; Feng, Y. More than 200 W random Raman fiber laser with ultra-short cavity length based on phosphosilicate fiber. *Opt. Lett.* **2019**, *44*, 1801–1804. [[CrossRef](#)]
23. Wang, Z.H.; Yan, P.; Huang, Y.S.; Tian, J.D.; Cai, C.; Li, D.; Yi, Y.Q.; Xiao, Q.R.; Gong, M.L. An Efficient 4-kW Level Random Fiber Laser Based on a Tandem-Pumping Scheme. *IEEE Photonics Technol. Lett.* **2019**, *31*, 817–820. [[CrossRef](#)]
24. Wang, Z.H.; Yu, W.L.; Tian, J.D.; Qi, T.C.; Li, D.; Xiao, Q.R.; Yan, P.; Gong, M.L. 5.1 kW Tandem-Pumped Fiber Amplifier Seeded by Random Fiber Laser with High Suppression of Stimulated Raman Scattering. *IEEE J. Quantum Electron.* **2021**, *57*, 6800109. [[CrossRef](#)]
25. Du, X.Y.; Zhang, H.W.; Ma, P.F.; Xiao, H.; Wang, X.L.; Zhou, P.; Liu, Z.J. Kilowatt-level fiber amplifier with spectral-broadening-free property, seeded by a random fiber laser. *Opt. Lett.* **2015**, *40*, 5311–5314. [[CrossRef](#)]
26. Babin, S.A.; Dontsova, E.I.; Kablukov, S.I. Random fiber laser directly pumped by a high-power laser diode. *Opt. Lett.* **2013**, *38*, 3301–3303. [[CrossRef](#)]
27. Du, X.Y.; Zhang, H.W.; Wang, X.L.; Zhou, P. Tunable random distributed feedback fiber laser operating at 1 μ m. *Appl. Opt.* **2015**, *54*, 908–911. [[CrossRef](#)]
28. Melkumov, M.A.; Bufetov, I.A.; Kravtsov, K.S.; Shubin, A.V.; Dianov, E.M. Lasing parameters of ytterbium-doped fibres doped with P₂O₅ and Al₂O₃. *Quantum Electron.* **2004**, *34*, 843–848. [[CrossRef](#)]
29. Glick, Y.; Sintov, Y.; Zuitlin, R.; Pearl, S.; Shamir, Y.; Feldman, R.; Horvitz, Z.; Shafir, N. Single-mode 230 W output power 1018 nm fiber laser and ASE competition suppression. *J. Opt. Soc. Am. B* **2016**, *33*, 1392–1398. [[CrossRef](#)]
30. Kurkov, A.S. Oscillation spectral range of Yb-doped fiber lasers. *Laser Phys. Lett.* **2007**, *4*, 93–102. [[CrossRef](#)]
31. Brilliant, N.A.; Lagonik, K. Thermal effects in a dual-clad ytterbium fiber laser. *Opt. Lett.* **2001**, *26*, 1669–1671. [[CrossRef](#)]
32. Wang, J.H.; Chen, G.; Zhang, L.; Hu, J.M.; Li, J.Y.; He, B.; Chen, J.B.; Gu, X.J.; Zhou, J.; Feng, Y. High-efficiency fiber laser at 1018 nm using Yb-doped phosphosilicate fiber. *Appl. Opt.* **2012**, *51*, 7130–7133. [[CrossRef](#)] [[PubMed](#)]

33. Xiao, H.; Zhou, P.; Wang, X.L.; Guo, S.F.; Xu, X.J. Experimental Investigation on 1018-nm High-Power Ytterbium-Doped Fiber Amplifier. *IEEE Photonics Technol. Lett.* **2012**, *24*, 1088–1090. [[CrossRef](#)]
34. Richardson, D.J.; Nilsson, J.; Clarkson, W.A. High power fiber lasers: Current status and future perspectives. *J. Opt. Soc. Am. B* **2010**, *27*, 63–92. [[CrossRef](#)]
35. Jauregui, C.; Limpert, J.; Tünnermann, A. High-power fibre lasers. *Nat. Photonics* **2013**, *7*, 861–867. [[CrossRef](#)]
36. Huang, Y.S.; Yan, P.; Wang, Z.H.; Tian, J.D.; Li, D.; Xiao, Q.R.; Gong, M.L. 2.19 kW narrow linewidth FBG-based MOPA configuration fiber laser. *Opt. Express* **2019**, *27*, 3136–3145. [[CrossRef](#)]
37. Jacquemet, M.; Mugnier, A.; Corre, G.L.; Goyat, E.; Pureur, D. CW PM multiwatts Yb-doped fiber laser directly emitting at long wavelength. *IEEE J. Sel. Top. Quantum Electron.* **2009**, *15*, 120–128. [[CrossRef](#)]

Disclaimer/Publisher's Note: The statements, opinions and data contained in all publications are solely those of the individual author(s) and contributor(s) and not of MDPI and/or the editor(s). MDPI and/or the editor(s) disclaim responsibility for any injury to people or property resulting from any ideas, methods, instructions or products referred to in the content.